# Signature of chaos and delocalization in a periodically driven many-body system: An out-of-time-order-correlation study

S. Ray,[1] S. Sinha,[1] and K. Sengupta[2]

[1]*Indian Institute of Science Education and Research, Kolkata, Mohanpur, Nadia 741246, India*

[2]*Theoretical Physics Department, Indian Association for the Cultivation of Science, Jadavpur, Kolkata 700032, India*

(Received 17 April 2018; published 27 November 2018)

We study out-of-time-order correlation (OTOC) for one-dimensional periodically driven hardcore bosons in the presence of Aubry-André (AA) potential and show that both the spectral properties and the saturation values of OTOC in the steady state of these driven systems provide a clear distinction between the localized and delocalized phases of these models. Our results, obtained via exact numerical diagonalization of these boson chains, thus indicate that OTOC can provide a signature of drive-induced delocalization, even for systems which do not have a well-defined semiclassical (and/or large $N$) limit. We demonstrate the presence of such a signature by analyzing two different drive protocols for hardcore boson chains leading to distinct physical phenomena and discuss experiments which can test our theory.

DOI: 10.1103/PhysRevA.98.053631

## I. INTRODUCTION

Identifying the signature of chaos in quantum systems is a longstanding issue [1,2] which has relevance for both its entanglement properties [3–5] and thermalization [6–9]. The typical fingerprint of chaos in a quantum system may be found in its spectral properties by invoking the Bohigas-Giannoni-Schmit (BGS) conjecture [10]. Recent studies however show that the out-of-time-order correlator (OTOC) provides an alternate and more direct way to quantify chaos, even in the interacting many-body systems [11–26]. Recent developments in the experimental techniques to measure the quantum correlations enable a direct investigation of the OTOC in trapped ions and spin systems [27,28]. For quantum systems with a well-defined semiclassical limit, OTOC provides a way to estimate the Lyapunov exponent which may be used to quantify the degree of chaos of the system [11,12]. Interestingly, application of this method in the Sachdev-Ye-Kitaev (SYK) model [29,30] provides an upper bound to this Lyapunov exponent, which is believed to have a connection with the information scrambling in black holes [31,32]. For the same reason, this method has its application in quantum information as well as in the study of the entanglement in strongly interacting quantum systems [33–36].

On the other hand, study of periodically driven many-body systems has regained interest after the recent experimental observation of drive-induced delocalization phenomena [37]. The study of an equivalent noninteracting model reveals that such delocalization phenomena stems from the underlying chaotic dynamics [38]. In this context OTOC turns out to be an ideal method to explore the connection between the delocalization and the underlying chaos in an interacting quantum system. Although the connection of OTOC with Lyapunov exponent has been explored in several condensed-matter systems [14–19], to the best our knowledge the delocalization transition from many-body localized (MBL) phases of quasiperiodic systems has not been investigated so far using OTOC.

The experimental realization of quasiperiodic system such as the Aubry-André (AA) model has become a test-bed to study single-particle [39] as well as MBL phenomena of strongly interacting systems [40–44], since the AA model exhibits localization transition in one dimension (1D) [45,46]. In a recent experiment the dynamics of many-body localized two-component fermions subjected to a driven AA model reveals delocalization phenomena controlled by the frequency of the drive [37]. Motivated by this experiment, in this work we consider a system of strongly interacting bosons in the presence of an AA potential subjected to two different types of periodic drives which have a different consequence on delocalization phenomena. Our goal is to study the commutator,

$$C(\beta_T, p) = \mathrm{Tr}[\hat{\rho}_{\beta_T}[\hat{W}(p), \hat{V}(0)]^\dagger[\hat{W}(p), \hat{V}(0)]], \quad (1)$$

calculated after the $p$th drive cycle using the thermal density matrix $\hat{\rho}_{\beta_T}$ at initial inverse temperature $k_B\beta_T$ (where $k_B$ is the Boltzmann constant), of suitable local unitary operators $\hat{W}(p) \equiv \hat{W}(t = pT)$ and $\hat{V}$, and to detect the delocalization transition in these driven systems from its behavior. We note that $C(\beta_T, p)$ is related to the OTOC, defined as

$$F(\beta_T, p) = \mathrm{Tr}[\hat{\rho}_{\beta_T}\hat{W}^\dagger(p)\hat{V}^\dagger(0)\hat{W}(p)\hat{V}(0)] \quad (2)$$

via $C(\beta_T, p) = 2(1 - \mathrm{Re}[F(\beta_T, p)])$. The last relation holds for operators $\hat{W}$ and $\hat{V}$ that satisfy $\hat{W}^\dagger\hat{W} = \hat{V}^\dagger\hat{V} = \hat{I}$; we shall always focus on such operators here.

Since in the semiclassical limit the Lyapunov exponent of the corresponding quantum system can be estimated from the unequal time commutator of conjugate dynamical variables [18], it is natural to expect that $C(\beta_T, p)$ would capture thermalization and underlying chaos in a quantum many-body system and thereby distinguish between its MBL and ergodic phases. In this work, by carrying out a detailed study of properties of $C(\beta_T, p)$ related to the OTOC for two

 

periodically driven boson models in the presence of an Aubry-André potential, we show that this is indeed the case. We discuss the dependence of the $C(\beta_T, p)$ on the time period $T$ of the drive and show that both its saturation value and spectral properties can distinguish between MBL and ergodic phases; our results thus show that these quantities can serve as an indicator of delocalization transition even for systems with no obvious semiclassical or large $N$ limit and thus with no clear definition of Lyapunov exponents. The unequal time commutator can also be useful to study the localization length since it involves the local operators and thereby contains the information of the spatial correlation. Moreover, recent experiments on the measurement of OTOC in the nonintegrable systems [27,28] opens up the possibility for a direct study of chaos in driven systems. Thus we believe that our method is much more experimentally relevant as well suitable to capture alongside the crossover from MBL to thermal phase induced by periodic drive and the underlying chaos.

We construct the Floquet operator to generalize OTOC for stroboscopic dynamics and compare the behavior of $C(\beta_T, p)$ with the spectral properties of the Floquet operator, which is a standard method to identify delocalization transition. The most general Hamiltonian describing a system under periodic perturbation is given by

$$\hat{H}(t) = \hat{H}_0 + \hat{H}_1(t), \tag{3}$$

where $\hat{H}_0$ is the time-independent part and the time-dependent part satisfies $\hat{H}_1(t+T) = \hat{H}_1(t)$, where $T$ is driving time period. The corresponding Floquet operator is $\hat{\mathcal{F}} = \hat{\mathcal{T}} e^{-i\int_{t_0}^{t_0+T} \hat{H}(t)dt/\hbar}$, where $\hat{\mathcal{T}}$ is the time ordering operator and the initial time $t_0 \in [0, T]$ gives a shift in time from $t = 0$, and the corresponding Floquet operators are related by a unitary transformation. The Floquet quasienergies do not depend on the choice of $t_0$ [47]; moreover, we checked that after long-time stroboscopic dynamics, the steady-state value of the observables remains unchanged under such shifts in initial time. Therefore in our study we set $t_0 = 0$. Due to the unitarity of $\hat{\mathcal{F}}$, the eigenvalue equation can be written as $\hat{\mathcal{F}}|\psi_\nu\rangle = e^{-i\phi_\nu}|\psi_\nu\rangle$, where $\phi_\nu$ and $|\psi_\nu\rangle$ are the $\nu$th eigenphase and eigenstate of $\hat{\mathcal{F}}$, respectively. The unequal time commutator $C(\beta_T, p)$, consisting of two unitary operators $\hat{W}$ and $\hat{V}$, after the $p$th drive cycle is given by Eq. (1) with $\hat{W}(p) = \hat{\mathcal{F}}^{\dagger p}\hat{W}(0)\hat{\mathcal{F}}^{p}$. In what follows, we describe two physical models and analyze the effect of the drive from the properties of Floquet operator and OTOC.

## II. MODEL I

We consider a periodically driven system of hardcore bosons at half filling within tight binding approximation and nearest neighbor (NN) interaction given by the Hamiltonian

$$\hat{H}_0 = -J\sum_l (\hat{b}_l^\dagger \hat{b}_{l+1} + \text{H.c.}) + \mathcal{V}\sum_l \hat{n}_l\hat{n}_{l+1}, \tag{4a}$$

$$\hat{H}_1(t) = \lambda[1 + \epsilon f(\omega t)]\sum_l \cos(2\pi\beta l)\hat{n}_l, \tag{4b}$$

where $\hat{b}_l^\dagger$ and $\hat{n}_l = \hat{b}_l^\dagger\hat{b}_l$ are the creation and the density operators of the bosons at the $l$th lattice site, respectively, $J$ is the hopping amplitude, $\mathcal{V}$ is the strength of the nearest-neighbor interaction, $\lambda$ denotes the amplitude of the quasiperiodic potential, and $\beta = (\sqrt{5}-1)/2$. For simplicity we consider a square pulse protocol, i.e., $f(\omega t) = 1$ for $(n-1)T \leqslant t < (n-1/2)T$ and $f(\omega t) = -1$, otherwise, where $n$ is an integer and the driving frequency is $\omega = 2\pi/T$. In the rest of the paper, we set $\hbar = 1$, all energies (times) are measured in units of $J(1/J)$, and we consider the inverse temperature $\beta_T = 0.1, \lambda = 3$, and $\epsilon = 0.47$ such that the time-independent Hamiltonian represents the localized regime of the AA model and drive induces mixing with the delocalized regime.

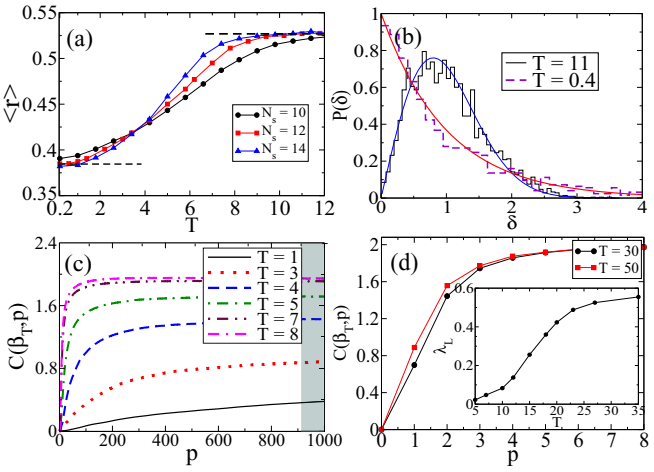


FIG. 1. (a) $\langle r\rangle$ is shown as function of $T$. (b) The spacing distributions of $\delta_\nu$'s for two typical values of $T$ are plotted; the corresponding probability distributions are shown by solid curves. (c) $C(\beta_T, p)$ is plotted with number of drives $p$, keeping the spatial distance fixed at $|l - l'| = 9$ for different values of driving time period $T$. The linear growth in the delocalized regime (for higher $T$ values) is shown in (d). In the inset the variation of $\lambda_L$ is shown as a function of $T$. The other parameters for this plot are $\lambda = 3, \epsilon = 0.47$, $\mathcal{V} = 0.1$, and $\beta_T = 0.1$.

We first find out the eigenphases $\phi_\nu$ of the corresponding Floquet operator and order them in $[-\pi, \pi]$. To quantify the degree of delocalization as well as to identify the change in the corresponding spectral statistics, we calculate the ratio between the consecutive level spacing, $r_\nu = \min(\delta_{\nu+1}, \delta_\nu)/\max(\delta_{\nu+1}, \delta_\nu)$, where $\delta_\nu = \phi_{\nu+1} - \phi_\nu$. We compute the average level spacing ratio $\langle r\rangle$; in the localized regime, $\langle r\rangle \approx 0.386$, signifying that the normalized spacing distribution follows Poisson statistics. In contrast, in the delocalized regime, $\langle r\rangle \approx 0.527$ corresponds to the orthogonal class of random matrix theory (RMT) [48–50]. From Fig. 1(a) we see that the value of $\langle r\rangle$ gradually increases from 0.386 and reaches a value of 0.527 with the increase in time period $T$, indicating the thermalization induced by the periodic drive. To compute the corresponding spacing distribution $P(\delta)$ of the eigenphases $(\phi_\nu)$, we follow the standard procedure as outlined in [1] in order to keep $\int P(\delta)d\delta = 1$ and $\int \delta P(\delta)d\delta = 1$. In Fig. 1(b) the spacing distributions are shown for two different values of the time period $T$ corresponding to the localized and delocalized regime.

Next we investigate the time evolution of the commutator $C(\beta_T, p)$ constructed from equivalent local Pauli spin

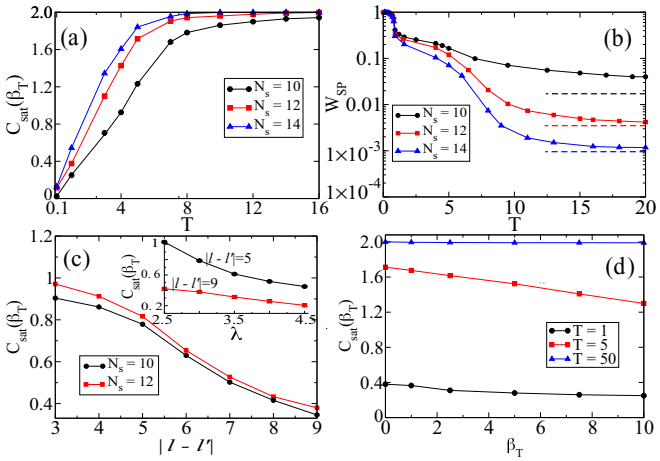


FIG. 2. Variation of $C_{\rm sat}(\beta_T)$ and the time-averaged survival probability $W_{SP}$ are shown as a function of $T$ for different system sizes $N_s$ in (a) and (b), respectively. The horizontal dashed lines denote the GOE value of $W_{SP} \sim 3/\mathcal{D}$. (c) $C_{\rm sat}(\beta_T)$ is plotted with $|l - l'|$ for $\lambda = 3$. In the inset variation of $C_{\rm sat}(\beta_T)$ is shown with increasing $\lambda$ for different $|l - l'|$. We set $N_s = 12$, $T = 1$. (d) Temperature dependence of $C_{\rm sat}(\beta_T)$ is shown.

operators $\hat{W} = \hat{\sigma}_z^l$ and $\hat{V} = \hat{\sigma}_z^{l'}$, where $\hat{\sigma}_z^l = 2\hat{n}_l - 1$ and $\hat{\sigma}_z^{l'} = 2\hat{n}_{l'} - 1$, $l$ and $l'$ being the site indices. Deep inside the MBL phase (for small $T$), due to the suppression of the kinetic energy, $\hat{\sigma}_z^l$ approximately commutes with the time-averaged Hamiltonian governing the physics of the MBL phase, resulting in a very slow growth of $C(\beta_T, p)$. Such a behavior has also been supported from the dynamics using a random matrix model discussed in Sec. III. Another feature of the MBL phase is the power-law decay of the OTOC, $|F(\beta_T, p)|$, with the number of drive $p$ [20] as illustrated in Fig. 8(a). On the other hand, the kinetic energy term becomes significant in the delocalized regime, which gives rise to exponential decay of the OTOC [as shown in Fig. 8(b)], resulting in a faster growth of the unequal time commutator $C(\beta_T, p)$. In Fig. 1(c) we have shown the stroboscopic time evolution of $C(\beta_T, p)$ for different driving time periods $T$. We observe that unlike the large-$N$ models, there is no such scrambling phenomena observed in this driven system in the delocalized regime and $C(\beta_T, p)$ grows almost linearly with the number of drives $p$, as depicted in Fig. 1(d). This is apparently due to the fact that the driving time period is much larger compared to the typical scrambling timescale; therefore the stroboscopic time evolution cannot capture this phenomena. Further, we fit such faster growth of $C(\beta_T, p)$ with a function $C_{\rm sat}(\beta_T)(1 - e^{-p\lambda_L})$, where $\lambda_L$ represents the growth rate and increases with increasing $T$, as shown in the inset of Fig. 1(d).

From Fig. 1(c), it turns out that $C(\beta_T, p)$ saturates eventually in the stroboscopic evolution; the saturation value $C_{\rm sat}(\beta_T) = \lim_{p\to\infty} C(\beta_T, p)$ increases with the driving time period $T$ and finally, for large $T$ it saturates to the value $C_{\rm sat}(\beta_T) \sim 2$. We performed a temporal averaging over the shaded region of Fig. 1(c), as well took ∼50 disorder realizations to obtain $C_{\rm sat}(\beta_T)$, and plotted as a function of $T$ in Fig. 2(a) for different system sizes. The behavior of $C_{\rm sat}(\beta_T)$ resembles the variation of $\langle r \rangle$ and therefore can capture the crossover from MBL to thermal phase with increasing time period $T$. It can be noted that for small $T$, say $T \sim 0.1$, as well as for large $T$ the value of $C_{\rm sat}(\beta_T)$ hardly depends on the system sizes [see Fig. 2(a)]. In the intermediate regime, say $T \sim 1 - 8$, $C_{\rm sat}(\beta_T)$ changes appreciably with $N_s$, which is atypical of any crossover phenomena. However, we note that the qualitative behavior of $C_{\rm sat}(\beta_T)$ as a function of $T$ remains similar for different system sizes, as shown in Fig. 2(a). We further observe that the finite-size effect becomes progressively smaller with increasing $N_s$; the value of $C_{\rm sat}(\beta_T)$ obtained for $N_s = 14$ is within 10% of the asymptotic value of $C_{\rm sat}(\beta_T)$ for $1/N_s \to 0$ (see Appendix C for details). Thus the crossover phenomena from MBL to thermal phase by tuning the driving time period $T$ is robust against the system sizes. Moreover, we find that for intermediate values of $T$ near the MBL phase ($T \sim 1$), there is an interplay between the localization length and the distance $|l - l'|$ between the local operators which can be qualitatively understood as follows. By decreasing the value of $|l - l'|$, the distance between the local operators become comparable to the localization length, resulting in a strong enhancement of $C_{\rm sat}(\beta_T)$ as illustrated in Fig. 2(c). To check the consistency of the result we have performed such numerical analysis for two different system sizes. The effect of localization length on $C_{\rm sat}(\beta_T)$ can also be understood from the dependence of $C_{\rm sat}(\beta_T)$ on $\lambda$. With increasing value of $\lambda$, the localization length decreases, leading to a decrease in $C_{\rm sat}(\beta_T)$ as depicted in the inset of Fig. 2(c). For larger values of $|l - l'|$, such dependence turns out to be very small [see the inset of Fig. 2(c)]. This is because $|l - l'|$ is already large compared to the localization length, and thus further increase in $\lambda$ does not have much effect on $C_{\rm sat}(\beta_T)$. We further investigate the temperature dependence of $C_{\rm sat}(\beta_T)$. For both MBL (small $T$) and the thermal phase (larger $T$), $C_{\rm sat}(\beta_T)$ has hardly any dependence on $\beta_T$; however, for intermediate values of $T$, $C_{\rm sat}(\beta_T)$ varies significantly with $\beta_T$ as shown in Fig. 2(d). Finally, in the delocalized regime $C_{\rm sat}(\beta_T)$ becomes temperature scale independent and attains the maximum value of 2, signifying the infinite temperature thermalization in driven systems [51–55].

The crossover to a delocalized phase can also be captured from the survival probability [56–59] of an initially prepared state in the coarse of time evolution analogous to the dynamics of an "imbalance factor" measured in the experiments to identify the delocalization transition [40–44]. In the dynamical evolution we choose the initial state $|\Psi(0)\rangle$ to be the ground state of the undriven Hamiltonian. During the stroboscopic time evolution in the presence of drive the survival probability of the initial state can be computed from $W_{SP}(p) = |\langle\Psi(0)|\hat{\mathcal{F}}^p|\Psi(0)\rangle|^2$. In the MBL phase $W_{SP}$ remains close to unity, whereas it decays in the delocalized regime. We compute the time-averaged value of $W_{SP}$ (obtained for $p \simeq 1000$ in our numerics) and depict its variation as a function of $T$ for different system sizes in Fig. 2(b). Well inside the delocalized regime $W_{SP}$ saturates to $\sim 3/\mathcal{D}$, which is in accordance with the RMT prediction [57], $\mathcal{D}$ being the dimension of the Hilbert space.

In order to understand the physics behind the decay of the survival probability, we calculate the overlap of the Floquet states with the eigenstates of the undriven Hamiltonian. We compute the quantity $c_{\alpha\nu} = \langle\psi_\nu|v_\alpha\rangle$, where $|v_\alpha\rangle$ is the

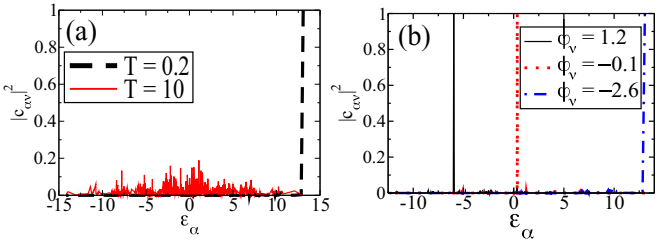


FIG. 3. (a) The overlap $|c_{\alpha\nu}|^2$ is shown as a function of $\epsilon_\alpha$ for a representative $\phi_\nu$ corresponding to the lowest eigenmode of $\hat{\mathcal{F}}$. (b) The same has been plotted for $T = 0.2$ and the eigenmodes corresponding to lowest, middle, and upper Floquet band.

eigenstate corresponding to the $\alpha$th eigenmode of the undriven Hamiltonian. In Figs. 3(a) and 3(b) we have shown $|c_{\alpha\nu}|^2$ corresponding to the Floquet state with eigenphase $\phi_\nu$ as a function of the eigenenergies $\epsilon_\alpha$ of the undriven Hamiltonian. We observe that in the small $T$ regime typically the Floquet states have maximal overlap with one of the eigenstates of the undriven Hamiltonian indicating localization, whereas in the delocalized regime (for higher $T$) the overlap function $|c_{\alpha\nu}|^2$ spreads over all the eigenmodes $|v_\alpha\rangle$. This observation indicates that in the localized regime, the dominating contributions come from the diagonal elements of the local operators $\hat{\sigma}_z^l$ in the Floquet basis. The saturation value of $F$ with $\hat{W} = \hat{V} = \hat{\sigma}_z^l$ is independent of $l$ and can be approximated by

$$F(\beta_T, p \to \infty) = \sum_{\alpha,\nu} \rho_{\beta_T}^{\alpha} |c_{\alpha\nu}|^2 s_{\nu\nu}^4 , \tag{5}$$

where $\rho_{\beta_T}^{\alpha} = e^{-\beta_T \epsilon_\alpha} / \sum_\alpha e^{-\beta_T \epsilon_\alpha}$ are elements of the initial thermal density matrix, $c_{\alpha\nu} = \langle v_\alpha | \psi_\nu \rangle$, and $s_{\nu\nu} = \langle \psi_\nu | \hat{\sigma}_z | \psi_\nu \rangle$ (see Appendix A for detail derivation). This approximate analytical formula surprisingly agrees well with the results obtained from the full stroboscopic dynamics even for large $T$, as illustrated in Fig. 4. From the above expression it can also be noted that in the delocalized regime the saturation value $C_{\rm sat}(\beta_T)$ becomes independent of temperature due to the spreading of the overlap function $|c_{\alpha\nu}|^2 \sim 1/\mathcal{D}$. Away from the ergodic phase, $C_{\rm sat}(\beta_T)$ exhibits temperature dependence, which becomes significant for the intermediate values of $T$ as depicted in Fig. 2(d) (also see Appendix A).

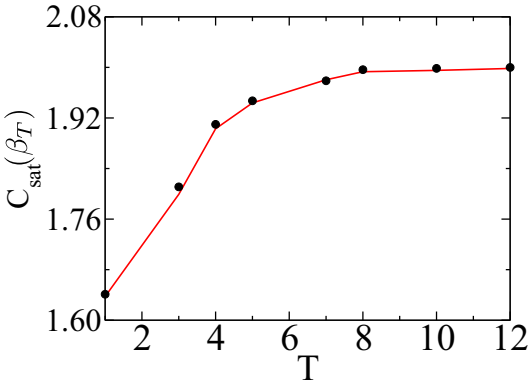


FIG. 4. $C_{\rm sat}(\beta_T)$ is shown as a function of $T$ for $l = l'$. The solid line is obtained from Eq. (5), and the circles represent the values obtained from the full stroboscopic time evolution. All other parameters are the same as in Fig. 1.

## III. EVOLUTION UNDER THE GAUSSIAN ORTHOGONAL ENSEMBLE MATRIX

In this section we discuss the stroboscopic dynamics governed by a model Hamiltonian consisting of a mixture of random matrix of Gaussian orthogonal ensemble (GOE) class and a Poisson matrix [60]. The Hamiltonian describing a mixed random matrix ensemble is given by

$$\hat{H}_R = \hat{H}_P + \bar{\lambda} \hat{H}_G / \sqrt{\mathcal{D}} , \tag{6}$$

where $\hat{H}_P$ is a random banded matrix exhibiting Poisson level spacing distribution, $\hat{H}_G$ is a GOE matrix, and $\mathcal{D}$ is the size of the matrix. In what follows we construct the Floquet operator $\hat{\mathcal{F}} = e^{-i\hat{H}_R T}$ and study its spectral properties as well as the dynamics governed by $\hat{\mathcal{F}}$. We note that here $\bar{\lambda}$ is a tuning parameter, and in the limit $\bar{\lambda} \to 0$, $\hat{H}_R$ is a Poisson matrix, whereas for $\bar{\lambda} \gg 1$, $\hat{H}_R$ resembles a GOE matrix.

*Spectral statistics.* From the eigenvalue equation $\hat{\mathcal{F}}|\psi_\nu\rangle = e^{-i\phi_\nu}|\psi_\nu\rangle$, we first compute the eigenphases $\phi_\nu$ corresponding to the eigenmode $|\psi_\nu\rangle$. We compute the average level spacing ratio $\langle r \rangle$ as defined in the main text and plot it as a function of $\bar{\lambda}$ in Fig. 5(a). For small $\lambda$, $\langle r \rangle \sim 0.386$, indicating the Poisson distribution; further increase in $\bar{\lambda}$ results in an increase in $\langle r \rangle$ and finally saturates to ∼0.527, representing the GOE class of the corresponding spacing distribution as depicted in Fig. 5(a).

*OTO correlator.* To study the time evolution under $\hat{\mathcal{F}}$, we first construct the initial thermal density matrix as $\hat{\rho}_{\beta_T} = e^{-\beta_T \hat{H}_P}$ so as to start from a localized system and evolve it stroboscopically. We calculate the commutator $C(\beta_T, p)$ and plot it as a function of $p$ for different values of $\bar{\lambda}$ in Fig. 5(b). It can be noted that the growth rate of $C(\beta_T, p)$ as well as the saturation value $C_{\rm sat}(\beta_T)$ obtained after sufficient number of drives increases with increasing $\bar{\lambda}$. This is further illustrated

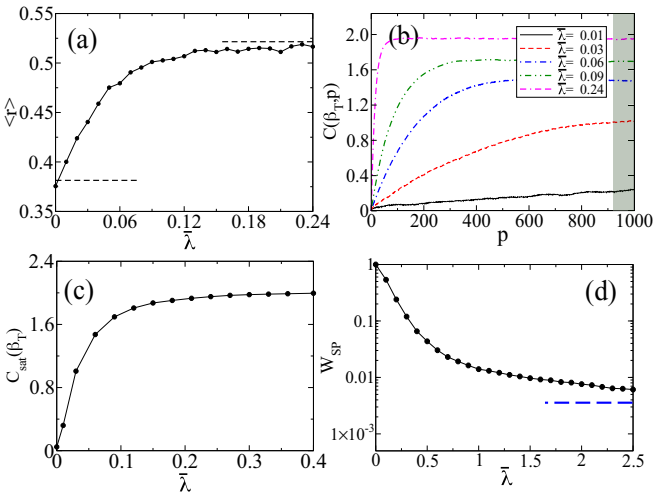


FIG. 5. (a) $\langle r \rangle$ as a function of $\bar{\lambda}$. (b) Stroboscopic time evolution of $C(\beta_T, p)$ for different values of $\bar{\lambda}$. Saturation value $C_{\rm sat}(\beta_T)$ and time-averaged $W_{SP}$ are plotted as a function of $\bar{\lambda}$ in (c) and (d). We have considered $\mathcal{D} = 924$.

in Fig. 5(c), where we have shown $C_{\rm sat}(\beta_T)$ as a function of $\bar{\lambda}$.

*Survival probability.* We further compute the survival probability of an initially prepared excited state which has been considered to be an eigenstate of $\hat{H}_P$. In Fig. 5(d) we have plotted the long-time-averaged value of $W_{SP}$ as a function of $\bar{\lambda}$. For small $\bar{\lambda}$ corresponding to the localized regime $W_{SP} \sim 1$ and with increasing $\bar{\lambda}$, survival probability reaches to the GOE value $\sim 3/\mathcal{D}$, as depicted by the dashed line in Fig. 5(d).

We note that the behavior of $\langle r\rangle$, $C_{\rm sat}(\beta_T)$, and $W_{SP}$ is similar to what we obtained above in Sec. II, where $T$ plays a similar role as $\bar{\lambda}$. It further strengthens our conclusions about the crossover from MBL to thermal phase by tuning the driving time period as captured from the above-mentioned measures. Since such an analysis is independent of the system Hamiltonian, therefore it reveals a more generic feature of such drive-induced delocalization phenomena.

## IV. MODEL II

In the second case we consider a periodic tilting of the lattice by applying an electric field which can be generated from a time-dependent vector potential [38]. In the presence of such driving, the system of strongly interacting bosons in a quasiperiodic potential can be described by the Hamiltonian

$$\hat{H}_0 = \sum_l [-J(\hat{b}_l^\dagger \hat{b}_{l+1} + \text{H.c.}) + \mathcal{V}\hat{n}_l\hat{n}_{l+1} + \lambda\cos(2\pi\beta l)\hat{n}_l], \quad \hat{H}_1(t) = E(\omega t)a\sum_l l\hat{n}_l\,, \quad (7)$$

where $a$ is the lattice spacing, and $E$ is the applied electric field which can be generated from a time-dependent vector potential $A(\omega t) = \Delta g(\omega t)/a$ using $E = -\partial_t A$, $\Delta$ being the driving amplitude. Considering $g(\omega t)$ to be a periodic triangular pulse with period $2\pi$, the resulting electric field is given by

$$E(\omega t) = -\frac{4\Delta}{aT}, \quad (n-3/4)T \leqslant t < (n-1/4)T$$
$$= \frac{4\Delta}{aT}, \quad \text{otherwise}, \quad (8)$$

where $n$ is an integer and the driving frequency is $\omega = 2\pi/T$. Such a drive gives rise to a nontrivial effect on the localization phenomena, which has been explored in [38]. In the noninteracting limit of the above model, it has been shown that there is a domain of frequency interval within which there appears a delocalized Floquet band which stems from the underlying chaotic dynamics of the equivalent classical model [38]. This is a counterintuitive scenario, since such a drive in the absence of quasiperiodic potential leads to the suppression of kinetic energy of the time-averaged Hamiltonian [61–65] and hence is expected to favor localization [66]. To explore such phenomena and its connection with the underlying chaos in the interacting many-body system, we now follow a similar procedure as outlined in *Model I*.

First we analyze the Floquet spectrum $\phi_\nu$ and compute the average level spacing ratio $\langle r\rangle$ to characterize the delocalized as well as the localized phase. In Fig. 6(a) we have shown $\langle r\rangle$ as a function of driving time period $T$. In both the small- and large-$T$ regime $\langle r\rangle \sim 0.386$, indicating the localized Floquet states; the corresponding spacing distribution of the eigenphases exhibits Poisson distribution as shown in the inset of Fig. 6(a). On the other hand, in the intermediate regime $\langle r\rangle$ increases with increasing $T$ and shows a peak at $T \sim 25$, exhibiting the level repulsion in the corresponding spacing distribution as depicted in the inset of Fig. 6(a). We further compute $C_{\rm sat}(\beta_T)$ and plot it as a function of $T$ in Fig. 6(b). We see that $C_{\rm sat}(\beta_T)$ shows a maximum at $T \sim 25$ and decreases on both sides, resembling the nonmonotonic behavior of $\langle r\rangle$. Although the peak values of both quantities $\langle r\rangle$ and $C_{\rm sat}(\beta_T)$ are less than those of the GOE limit, it clearly distinguishes the MBL phase and indicates an approach to thermalization.

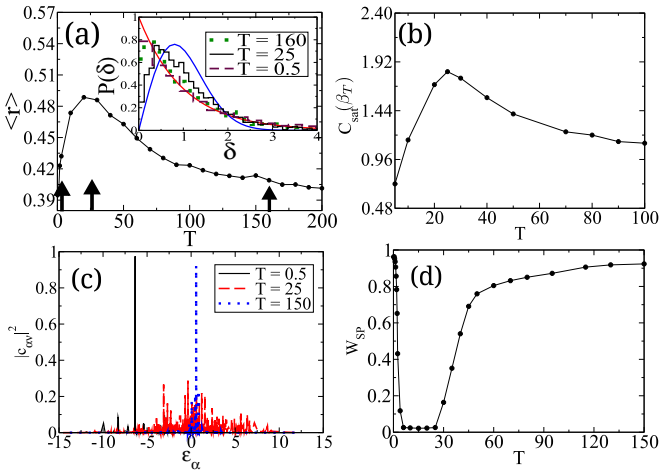


FIG. 6. (a) $\langle r\rangle$ as a function of $T$ is shown. In the inset the distribution of the spacing $\delta_\nu$'s are shown for three typical values of $T$; the corresponding probability distributions are shown by the solid lines. $C_{\rm sat}(\beta_T)$ and $W_{SP}$ are plotted with $T$ in (b) and (d), respectively. (c) The overlap $|c_{\alpha\nu}|^2$ is shown as a function of $\epsilon_\alpha$ for a representative $\phi_\nu$ corresponding to the lowest eigenmode of $\hat{\mathcal{F}}$. The other parameters are $\lambda = 3$, $\Delta = 1$, $\mathcal{V} = 0.1$, and $\beta_T = 0.1$.

To explore the connection of underlying chaos with the delocalization of the many-body Floquet states, we compute the overlap function $|c_{\alpha\nu}|^2$ and plot it in Fig. 6(c) for different values of $T$. For small as well as for larger values of $T$, $|c_{\alpha\nu}|^2$ shows a maximum overlap with one of the eigenmodes of the undriven Hamiltonian in Eq. (7), indicating localization, whereas for intermediate values of $T \sim 25$ the overlap function spreads over the eigenmodes $|\nu_\alpha\rangle$ showing delocalization of the Floquet states. The peak in $C_{\rm sat}(\beta_T)$ and the spreading of the overlap function $|c_{\alpha\nu}|^2$ indicates that such delocalization phenomena within an intermediate domain of $T$ is a manifestation of the underlying chaos in the many-body system. The delocalization of the Floquet states further results in the decay of survival probability $W_{SP}$ around $T \sim 25$. In Fig. 6(d) we have shown the behavior of $W_{SP}$ as a function of $T$; the dip around $T \sim 25$ indicates delocalization, and the minimum value approaches the GOE limit. Such a domain of $T$ where delocalized Floquet states appear can also be captured from the entanglement entropy and has been illustrated in [38].

## V. STATISTICS OF OTOC

Next, we focus on the statistics of OTOC motivated by a recent observation that the level spacing distribution of the OTOC corresponding to a single-particle chaotic Hamiltonian exhibits a level repulsion analogous to the Gaussian unitary (GUE) universality class [19]. In what follows we test the statistics obtained from the eigenmodes of the OTOC operator $\hat{F} = \hat{W}^\dagger(p)\hat{V}^\dagger(0)\hat{W}(p)\hat{V}(0)$ to distinguish the delocalization and thermalization phenomena in a driven many-body system. We compute the operator $\hat{F}$ after a sufficient number of drives and calculate the structural entropy $S^\mu_{str}$ of the $\mu$th eigenmode $|e_\mu\rangle$ of $\hat{F}$, defined as [67,68]

$$S^\mu_{str} = -\sum_\chi |c^\mu_\chi|^2 \ln |c^\mu_\chi|^2 - \ln \xi_\mu, \tag{9}$$

where $c^\mu_\chi = \langle \chi | e_\mu \rangle$ is the overlap of $|e_\mu\rangle$ with the computational basis $|\chi\rangle$, and $\xi_\mu = 1/\sum_\chi |c^\mu_\chi|^4$ is the corresponding inverse participation ratio (IPR). For the eigenvectors of the random matrices of the Gaussian unitary class, the average structural entropy $S_{str}$ approaches a universal value $\sim$0.27 [69,70] independent of the dimensionality of the Hilbert space. In Figs. 7(a) and 7(c) the variation of $S_{str}$ with increasing $T$ is shown for both models I and II, respectively. The corresponding distribution of the structural entropy $P(S^\mu_{str})$ is depicted in Figs. 7(b) and 7(d) for different values of $T$ belonging to the localized regime and the delocalized regime of both models. We notice that in the regime where thermalization occurs, structural entropy is sharply peaked at the value $\sim$0.27, indicating the GUE universality class. On the other hand in the localized regime, the peak vanishes and $P(S^\mu_{str})$ shows a broad distribution with increasing width $\Delta S_{str} = \sqrt{\langle S^{\mu 2}_{str}\rangle - \langle S^\mu_{str}\rangle^2}$ shown by the error bars. This observation confirms that the statistics of OTOC can be an alternate method to detect delocalization in a strongly interacting driven system.

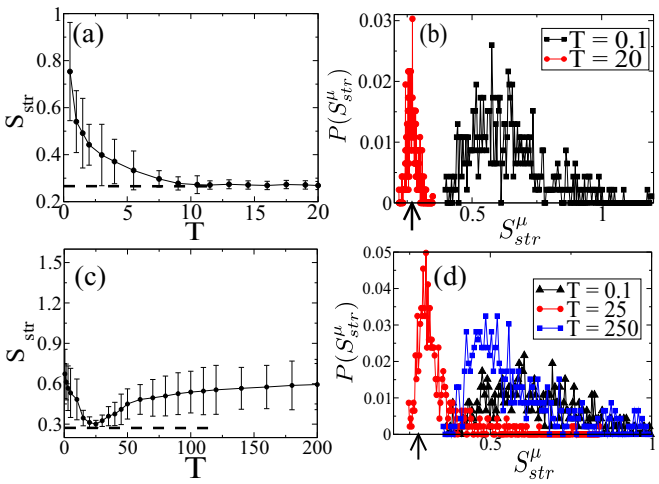


FIG. 7. (a) $\langle S_{str}\rangle$ is plotted with increasing $T$ corresponding to model I. The error bars indicate the width $\Delta S_{str}$ of the distribution of structural entropy $P(S^\mu_{str})$, shown in (b) for typical values of $T$ mentioned therein. The horizontal dashed lines in (a) and the arrow head in (b) indicate the GUE value of the structural entropy. The same has been plotted in (c) and (d) for model II.

## VI. CONCLUSION

To summarize, we have studied the behavior of $C_{\rm sat}(\beta_T)$ related to OTOC to detect the delocalization of the MBL phase in a strongly interacting bosonic system in the presence of a quasiperiodic potential subjected to two types of periodic drives showing distinctly different phenomena. We have shown that the saturation value of the unequal time commutator $C_{\rm sat}(\beta_T)$, the survival probability $W_{SP}$, and the spectral property of the OTOC can efficiently distinguish between the MBL and the thermal regimes of such driven models, as well capture the crossover between the two phases, by tuning the driving time period $T$. We have also analyzed the temperature dependence of $C_{\rm sat}(\beta_T)$, which can be used in experiments to detect the crossover region. The spatial dependence of $C_{\rm sat}(\beta_T)$ can serve as a useful tool to estimate the localization length. Therefore $C_{\rm sat}(\beta_T)$ can be an ideal measure to capture MBL to thermal phase transition as well to capture the underlying chaos. Moreover, recent experiments on the measurement of OTOC in trapped ions and NMR systems [27,28] provide the way to calculate the saturation value $C_{\rm sat}(\beta_T)$ and can further be implemented to study such drive-induced delocalization in a system of strongly interacting bosons in periodically driven AA potential. The survival probability can be measured in experimentation from the decay of an initially prepared state of the system in a similar way as has been done to measure the "imbalance factor" in cold atom experiments [37,40–44]. In previously studied noninteracting AA models, under a similar driving protocol it has been shown that the drive-induced delocalization phenomena is connected with the chaotic dynamics of the corresponding classical model [38]. Our present study also confirms that the delocalization phenomena has a connection with the underlying chaotic dynamics of an interacting quantum system, even when a direct classical correspondence is absent. Our results thus provide an alternate approach to diagnose the chaos as well as its connection with the thermalization in driven interacting many-body systems and can be tested in experiments in a similar line of thought as in [27,28,37,40–44].

## ACKNOWLEDGMENTS

S.R. thanks A. Mirlin, I. Bloch, and U. Schneider for many insightful discussions.

## APPENDIX A: DERIVATION OF ANALYTICAL EXPRESSION OF OTOC FOR MODEL I

In this Appendix we sketch the derivation of Eq. (5) of the main text. The quantity $F(\beta_T, p)$ after $p$ cycles of the drive and at an initial inverse temperature $\beta_T$ is given by

$$\begin{aligned} F(\beta_T, p) &= \mathrm{Tr}[\hat{\rho}_{\beta_T}\hat{W}^\dagger(p)\hat{V}^\dagger(0)\hat{W}(p)\hat{V}(0)] \\ &= \frac{1}{Z}\sum_\alpha e^{-\beta_T \epsilon_\alpha}\mathcal{L}_\alpha, \end{aligned} \tag{A1}$$

where $\mathcal{L}_\alpha = \langle v_\alpha|\hat{W}^\dagger(p)\hat{V}^\dagger(0)\hat{W}(p)\hat{V}(0)|v_\alpha\rangle$, $\hat{W}(p) = \hat{\mathcal{F}}^{\dagger p}\hat{W}(0)\hat{\mathcal{F}}^p$, $\hat{\mathcal{F}}$ is the time evolution operator, $|v_\alpha\rangle$, $\epsilon_\alpha$ denotes eigenvectors and eigenvalues of $\hat{H}(t=0)$ [see Eq. (4) in the main text], and $Z = \sum_\alpha \exp(-\beta_T\epsilon_\alpha)$ is the corresponding partition function. We then decompose $\hat{\mathcal{F}}$ in terms of its eigenstates $|\psi_\nu\rangle$ and eigenenergies $\phi_\nu$ (as defined in the main text). A few lines of algebra yields

$$\mathcal{L}_\alpha = \sum_{\mu,\nu,\lambda,\mu'\nu'} c^*_{\alpha\mu}c_{\nu\alpha}e^{ip\chi T}\, W_{\mu\mu'}W_{\lambda\nu'}V_{\mu'\lambda}V_{\nu'\nu}\,. \quad \text{(A2)}$$

Here $c_{\alpha\nu} = \langle v_\alpha|\psi_\nu\rangle$ denotes the overlap function, $\chi = \phi_\mu + \phi_\lambda - \phi_{\mu'} - \phi_{\nu'}$, the driving time period is $T$, and $W_{\nu\nu'}$ denotes the matrix element of $\hat{W}(0)$ between Floquet eigenstates $|\psi_\nu\rangle$ and $|\psi_{\nu'}\rangle$. For $p\to\infty$, the contribution to $\mathcal{L}_\alpha$ is obtained from terms for which $\phi_\mu + \phi_\lambda = \phi_{\mu'} + \phi_{\nu'}$, leading to $\chi = 0$. Furthermore, numerically, we find that for $\hat{W} = \hat{V} = \hat{\sigma}_z$, these matrix elements have a maximal contribution from the diagonal terms. Thus we obtain $\langle\psi_\nu|\hat{\sigma}_z|\psi_{\nu'}\rangle \simeq s_{\nu\nu'}\delta_{\nu\nu'}$, resulting in the expression $\mathcal{L}_\alpha = |c_{\alpha\nu}|^2 s^4_{\nu\nu}$. Finally, we obtain

$$F(\beta_T, p\to\infty) = \frac{\sum_{\alpha,\nu} e^{-\beta_T\epsilon_\alpha}|c_{\alpha\nu}|^2 s^4_{\nu\nu}}{\sum_\alpha e^{-\beta_T\epsilon_\alpha}}\,, \quad \text{(A3)}$$

which is Eq. (5) of the main text.

We find that in the delocalized regime $|c_{\alpha\nu}|^2 \sim 1/\mathcal{D}$, where $\mathcal{D}$ is the dimension of the matrix. This results in the saturation value of $C_{\rm sat}(\beta_T) \sim 2$, indicating that such a driven system thermalizes to infinite temperature where $C_{\rm sat}(\beta_T)$ becomes independent of $\beta_T$. In contrast, away from the ergodic phase near delocalization, the saturation value of the OTOC increases with decreasing temperature, resulting in the decrease of $C_{\rm sat}(\beta_T)$ with increasing $\beta_T$, as illustrated in Fig. 2(d). Such a growth of OTOC with inverse temperature $\beta_T$ can be understood as follows. We first note that in Eq. (5), $\sum_\nu |c_{\alpha\nu}|^2 = 1$ for all $\alpha$; moreover, it can be checked numerically that $s^4_{\nu\nu} < 1$ for all $\nu$. Thus the quantity $\mathcal{L}_\alpha = \sum_\nu |c_{\alpha\nu}|^2 s^4_{\nu\nu} < 1$, which ensures the convergence of the numerator of Eq. (5), since $\epsilon_\alpha$ can always chosen to be positive without any loss of generality. In terms of $\mathcal{L}_\alpha$, one can write

$$F(\beta_T, p\to\infty) = \frac{\sum_\alpha e^{-\beta_T\epsilon_\alpha}\mathcal{L}_\alpha}{\sum_\alpha e^{-\beta_T\epsilon_\alpha}}\,. \quad \text{(A4)}$$

Using this expression, it is straightforward to see that

$$\frac{\partial F(\beta_T, p\to\infty)}{\partial\beta_T} = \frac{1}{Z^2}\sum_{\alpha\neq\alpha'} e^{-\beta_T(\epsilon_\alpha+\epsilon_{\alpha'})}\epsilon_\alpha\mathcal{L}_{\alpha'} > 0\,. \quad \text{(A5)}$$

Thus $F(\beta_T, p\to\infty)$ must increase with increasing $\beta_T$, leading to a decrease of $C_{\rm sat}(\beta_T)$ with $\beta_T$, as shown in Fig. 2(d).

## APPENDIX B: DECAY OF OTOC IN MBL AND THERMAL PHASE

In this Appendix we will study the stroboscopic evolution of the OTOC corresponding to model I. In Figs. 1(c) and 1(d) of the main text it has been shown that the growth rate of $C(\beta_T, p)$ is very small in the MBL phase, but on the other hand, $C(\beta_T, p)$ grows very fast in the delocalized regime. In contrast, the OTOC, $F(\beta_T, p)$, shows a very slow power-law decay in the MBL phase, as depicted in a logarithmic plot of the scaled quantity $\bar{F}(\beta_T, p) = (|F(\beta_T, p)| - |F_{\rm sat}(\beta_T)|)/(1 - |F_{\rm sat}(\beta_T)|)$ in Fig. 8(a), where $F_{\rm sat}(\beta_T) = \lim_{p\to\infty} F(\beta_T, p)$. On the other hand, for large driving time periods $T$ the OTOC decays exponentially fast and saturates to a vanishingly small value, as shown in Fig. 8(b).

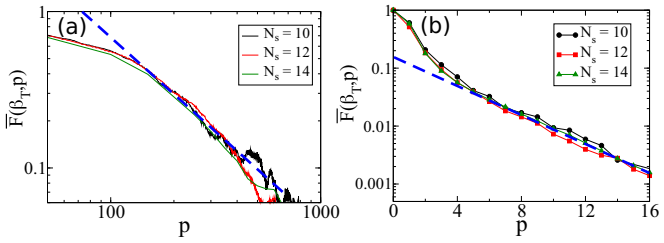


FIG. 8. The stroboscopic time evolution of $|F(\beta_T, p)|$ is shown in the localized regime for $T = 3$ in (a) and in the delocalized regime for $T = 50$ in (b). The dashed lines in (a) and (b) indicate the linear behavior in log-log plot and in semilog plot, respectively.

## APPENDIX C: FINITE-SIZE EFFECT ON $C_{\rm sat}(\beta_T)$

In this Appendix we have analyzed the effect of finite size of the system on $C_{\rm sat}(\beta_T)$. From Fig. 2(a) it can be noted that in the two extremes, for smaller $T \sim 0.1$ and for larger $T$, the value of $C_{\rm sat}(\beta_T)$ hardly depends on the system sizes. However, in the intermediate regime, say $T \sim 1$–$8$, $C_{\rm sat}(\beta_T)$ varies with different system sizes.

We note that although the value of $C_{\rm sat}(\beta_T)$ changes drastically by increasing the system size from $N_s = 8$ to $N_s = 10$, such changes in $C_{\rm sat}(\beta_T)$ due to system size become progressively smaller with increasing $N_s$, as depicted by the variation of $C_{\rm sat}(\beta_T)$ with $1/N_s$ in Fig. 9. We further fit such data with a fitting function $\bar{\alpha} + \bar{\beta}/N_s^{\bar{\gamma}}$; from the fitted values we obtained $\bar{\alpha} \sim 1.54$ (in limit $1/N_s \to 0$) corresponding to $T = 3$. We note that using the system size $N_s = 14$ we obtained the value of $C_{\rm sat}(\beta_T) \sim 1.37$, which is ~10% of the "thermodynamic limit."

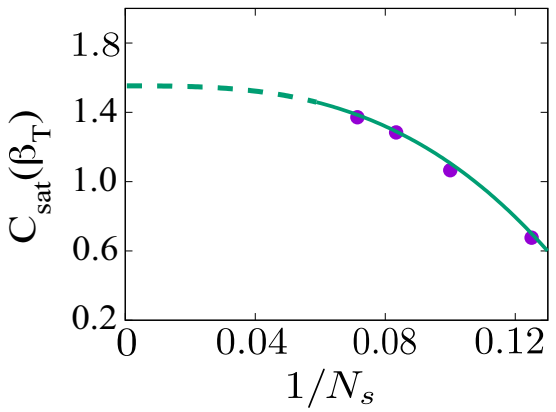


FIG. 9. $C_{\rm sat}(\beta_T)$ as a function of $1/N_s$ is plotted for $T = 3$ and $|l - l'| = 7$ for different system sizes $N_s$. Filled circles indicate the numerical data points, and the solid line represents the fitted curve. All other parameters are the same as in Fig. 1.

[1] F. Haake, *Quantum Signatures of Chaos* (Springer Science and Business Media, New York, 2013), Vol. 54.

[2] G. Casati, B. V. Chirikov, F. M. Izrailev, and J. Ford, Stochastic Behavior of a Quantum Pendulum Under A Periodic Perturbation, in *Stochastic Behavior in Classical and Quantum Hamiltonian Systems*, edited by G. Casati and J. Ford, Lecture Notes in Physics Vol. 93, (Springer, Berlin, 1979), pp. 334–352.

[3] S. Chaudhury, A. Smith, B. E. Anderson, S. Ghose, and P. S. Jessen, Nature (London) **461**, 768 (2009).

[4] C. Neill *et al.*, Nat. Phys. **12**, 1037 (2016).

[5] A. M. Kaufman, M. E. Tai, A. Lukin, M. Rispoli, R. Schittko, P. M. Preiss, and M. Greiner, Science **353**, 794 (2016).

[6] J. M. Deutsch, Phys. Rev. A **43**, 2046 (1991).

[7] M. Srednicki, Phys. Rev. E **50**, 888 (1994).

[8] F. Borgonovi, F. M. Izrailev, L. F. Santos, and V. G. Zelevinsky, Phys. Rep. **626**, 1 (2016).

[9] L. D'Alessio, Y. Kafri, A. Polkovnikov, and M. Rigol, Adv. Phys. **65**, 239 (2016).

[10] O. Bohigas, M. J. Giannoni, and C. Schmit, Phys. Rev. Lett. **52**, 1 (1984); J. Phys. Lett. **45**, 1015 (1984).

[11] A. I. Larkin and Y. N. Ovchinnikov, Zh. Eksp. Teor. Fiz. **55**, 2262 (1968) [Sov. Phys. JETP **28**, 1200 (1969)].

[12] D. A. Roberts and B. Swingle, Phys. Rev. Lett. **117**, 091602 (2016).

[13] K. Hashimoto, K. Murata, and R. Yoshii, J. High Energy Phys. 10 (2017) 138.

[14] B. Swingle and D. Chowdhury, Phys. Rev. B **95**, 060201(R) (2017).

[15] A. A. Patel, D. Chowdhury, S. Sachdev, and B. Swingle, Phys. Rev. X **7**, 031047 (2017).

[16] N. Y. Yao, F. Grusdt, B. Swingle, M. D. Lukin, D. M. Stamper-Kurn, J. E. Moore, and E. Demler, arXiv:1607.01801.

[17] A. Bohrdt, C. B. Mendl, M. Endres, and M. Knap, New J. Phys. **19**, 063001 (2017).

[18] E. B. Rozenbaum, S. Ganeshan, and V. Galitski, Phys. Rev. Lett. **118**, 086801 (2017).

[19] E. B. Rozenbaum, S. Ganeshan, and V. Galitski, arXiv:1801.10591.

[20] X. Chen, T. Zhou, D. A. Huse, and E. Fradkin, Ann. Phys. (Berlin) **529**, 1600332 (2017).

[21] M. Heyl, F. Pollmann, and B. Dońa, Phys. Rev. Lett. **121**, 016801 (2018).

[22] A. Das, S. Chakrabarty, A. Dhar, A. Kundu, D. A. Huse, R. Moessner, S. S. Ray, and S. Bhattacharjee, Phys. Rev. Lett. **121**, 024101 (2018).

[23] C.-J. Lin and O. I. Motrunich, Phys. Rev. B **97**, 144304 (2018).

[24] D. J. Luitz and Y. Bar Lev, Phys. Rev. B **96**, 020406(R) (2017).

[25] P. Bordia, F. Alet, and P. Hosur, Phys. Rev. A **97**, 030103(R) (2018).

[26] G. Zhu, M. Hafezi, and T. Grover, Phys. Rev. A **94**, 062329 (2016).

[27] M. Gärttner, J. G. Bohnet, A. Safavi-Naini, M. L. Wall, J. J. Bollinger, and A. M. Rey, Nat. Phys. **13**, 781 (2017).

[28] J. Li, R. Fan, H. Wang, B. Ye, B. Zeng, H. Zhai, X. Peng, and J. Du, Phys. Rev. X **7**, 031011 (2017).

[29] S. Sachdev and J. Ye, Phys. Rev. Lett. **70**, 3339 (1993).

[30] A. Kitaev, Hidden correlations in the Hawking radiation and thermal noise, talk given at Fundamental Physics Prize Symposium, 2014, http://online.kitp.ucsb.edu/online/joint98/kitaev/.

[31] S. H. Shenker and D. Stanford, J. High Energy Phys. 03 (2014) 067.

[32] J. Maldacena, S. H. Shenker, and D. Stanford, J. High Energy Phys. 08 (2016) 106.

[33] M. Gärttner, P. Hauke, and A. M. Rey, Phys. Rev. Lett. **120**, 040402 (2018).

[34] P. Hosur, X.-L. Qi, D. A. Roberts, and B. Yoshida, J. High Energy Phys. 02 (2016) 004.

[35] R. Fan, P. Zhang, H. Shen, and H. Zhai, Sci. Bull. **62**, 707 (2017).

[36] B. Swingle, G. Bentsen, M. Schleier-Smith, and P. Hayden, Phys. Rev. A **94**, 040302(R) (2016).

[37] P. Bordia, H. Lüschen, U. Schneider, M. Knap, and I. Bloch, Nat. Phys. **13**, 460 (2017).

[38] S. Ray, A. Ghosh, and S. Sinha, Phys. Rev. E **97**, 010101(R) (2018).

[39] G. Roati *et al.*, Nature (London) **453**, 895 (2008).

[40] M. Schreiber *et al.*, Science **349**, 842 (2015).

[41] J.-y. Choi *et al.*, Science **352**, 1547 (2016).

[42] P. Bordia, H. P. Lüschen, S. S. Hodgman, M. Schreiber, I. Bloch, and U. Schneider, Phys. Rev. Lett. **116**, 140401 (2016).

[43] H. P. Lüschen, P. Bordia, S. Scherg, F. Alet, E. Altman, U. Schneider, and I. Bloch, Phys. Rev. Lett. **119**, 260401 (2017).

[44] P. Bordia, H. Lüschen, S. Scherg, S. Gopalakrishnan, M. Knap, U. Schneider, and I. Bloch, Phys. Rev. X **7**, 041047 (2017).

[45] S. Aubry and G. André, Ann. Israel Phys. Soc. **3**, 133 (1980).

[46] C. Aulbach, A. Wobst, G. L. Ingold, P. Hänggi, and I. Varga, New J. Phys. **6**, 70 (2004).

[47] A. Lazarides, A. Das, and R. Moessner, Phys. Rev. Lett. **112**, 150401 (2014); **115**, 030402 (2015); Phys. Rev. E **90**, 012110 (2014).

[48] V. Oganesyan and D. A. Huse, Phys. Rev. B **75**, 155111 (2007).

[49] S. Iyer, V. Oganesyan, G. Refael, and D. A. Huse, Phys. Rev. B **87**, 134202 (2013).

[50] Y. Y. Atas, E. Bogomolny, O. Giraud, and G. Roux, Phys. Rev. Lett. **110**, 084101 (2013).

[51] L. D'Alessio and M. Rigol, Phys. Rev. X **4**, 041048 (2014).

[52] H. Kim, T. N. Ikeda, and D. A. Huse, Phys. Rev. E **90**, 052105 (2014).

[53] S. Ray, A. Ghosh, and S. Sinha, Phys. Rev. E **94**, 032103 (2016).

[54] A. Russomanno, R. Fazio, and G. E. Santoro, Europhys. Lett. **110**, 37005 (2015).

[55] N. Regnault and R. Nandkishore, Phys. Rev. B **93**, 104203 (2016).

[56] E. J. Torres-Herrera, A. M. García-García, and L. F. Santos, Phys. Rev. B **97**, 060303(R) (2018).

[57] E. J. Torres-Herrera, J. Karp, M. Távora, and L. F. Santos, Entropy **18**, 359 (2016).

[58] S. Lerma-Hernández, J. Chávez-Carlos, M. A. Bastarrachea-Magnani, L. F. Santos, and J. G. Hirsch, J. Phys. A: Math. Theor. **51**, 475302 (2018).

[59] L. F. Santos and E. J. Torres-Herrera, arXiv:1803.06012.

[60] S. Schierenberg, F. Bruckmann, and T. Wettig, Phys. Rev. E **85**, 061130 (2012).

[61] A. Eckardt, Rev. Mod. Phys. **89**, 011004 (2017).

[62] N. Goldman and J. Dalibard, Phys. Rev. X **4**, 031027 (2014).
[63] H. Lignier, C. Sias, D. Ciampini, Y. Singh, A. Zenesini, O. Morsch, and E. Arimondo, Phys. Rev. Lett. **99**, 220403 (2007).
[64] C. Sias, H. Lignier, Y. P. Singh, A. Zenesini, D. Ciampini, O. Morsch, and E. Arimondo, Phys. Rev. Lett. **100**, 040404 (2008).
[65] A. Eckardt, M. Holthaus, H. Lignier, A. Zenesini, D. Ciampini, O. Morsch, and E. Arimondo, Phys. Rev. A **79**, 013611 (2009).
[66] E. Bairey, G. Refael, and N. H. Lindner, Phys. Rev. B **96**, 020201(R) (2017).
[67] J. Pipek and I. Varga, Phys. Rev. A **46**, 3148 (1992).
[68] P. Jacquod and I. Varga, Phys. Rev. Lett. **89**, 134101 (2002).
[69] F. M. Izrailev, Phys. Rep. **196**, 299 (1990); **276**, 85 (1996).
[70] S. Ray, B. Mukherjee, S. Sinha, and K. Sengupta, Phys. Rev. A **96**, 023607 (2017).